Available online at www.sciencedirect.com
ScienceDirect
International Journal of Solids and Structures 45 (2008) 2233–2250
INTERNATIONAL JOURNAL OF SOLIDS AND STRUCTURES
www.elsevier.com/locate/ijsolstr

# Failure in notched tension bars due to high-temperature creep: Interaction between nucleation controlled cavity growth and continuum cavity growth

D.R. Hayhurst [a,*], J. Lin [b], R.J. Hayhurst [a]

[a] School of Mechanical, Aerospace and Civil Engineering, The University of Manchester, Sackville Street Building, P.O. Box 88, Manchester, M60 1QD, UK
[b] Department of Mechanical and Manufacturing Engineering, The University of Birmingham, Birmingham B15 2TT, UK

Received 23 July 2007; received in revised form 15 November 2007
Available online 15 December 2007

**Abstract**

For axi-symmetrically notched tension bars [Dyson, B.F., Loveday, M.S., 1981, Creep Fracture in Nimonic 80A under Tri-axial Tensile Stressing, In: Ponter A.R.S., Hayhurst, D.R. (Eds.), Creep in Structures, Springer-Verlag, Berlin, pp. 406–421] show two types of damage propagation are shown: for low stress, failure propagates from the outside notch surface to the centre-line; and for high stress, failure propagates from the centre-line to the outside notch surface. The objectives of the paper are to: identify the physics of the processes controlling global failure modes; and, describe the global behaviour using physics-based constitutive equations.

Two sets of constitutive equations are used to model the softening which takes place in tertiary creep of Nimonic 80A at 750 °C. Softening by multiplication of mobile dislocations is firstly combined, for low stress, with softening due to nucleation controlled creep constrained cavity growth; and secondly combined, for high stress, with softening due to continuum void growth. The Continuum Damage Mechanics, CDM, Finite Element Solver DAMAGE XX has been used to study notch creep fracture. Low stress notch behaviour is accurately predicted provided that the constitutive equations take account of the effect of stress level on creep ductility. High stress notch behaviour is accurately predicted from a normalized inverse cavity spacing $d/2\ell = 6$, and an initial normalized cavity radius $r_{hi}/\ell = 3.16 \times 10^{-3}$, where $2\ell$ is the cavity spacing, and $d$ is the grain size; however, the constants in the strain rate equation required recalibration against high stress notch data. A void nucleation mechanism is postulated for high stress behaviour which involves decohesion where slip bands intersect second phase grain boundary particles. Both equation sets accurately predict experimentally observed global failure modes.


*Keywords:* Creep rupture; Notched bars; Nucleation controlled and continuum cavity growth

* Corresponding author. Tel.: +44 161 306 3818; fax: +44 161 306 3803.
*E-mail address:* d.r.hayhurst@manchester.ac.uk (D.R. Hayhurst).

0020-7683/$ - see front matter © 2007 Elsevier Ltd. All rights reserved.
doi:10.1016/j.ijsolstr.2007.11.026

**Nomenclature**

*Stress*

$\sigma_1$ Uni-axial stress
$\sigma_{ij}$ Stress tensor
$\sigma_e(=3\sigma_{ij}\sigma_{ij}/2)^{1/2}$ Effective stress
$\sigma_0$ Normalizing stress
$\tilde{S}_{ij}$ Stress deviation tensor
$\tilde{J}_1$ Normalized first stress invariant
$\Sigma_{ij}(=\sigma_{ij}/\sigma_0)$ Normalized stress tensor
$S_{ij}(=\tilde{S}_{ij}/\sigma_0)$ Normalized stress deviation tensor
$\Sigma_e(=\sigma_e/\sigma_0)$ Normalized effective stress

*Strain*

$\dot{\varepsilon}_1$ Uni-axial creep strain rate
$\dot{\varepsilon}_{ij}$ Creep strain rate tensor
$\dot{\varepsilon}_o(=A=P)$ Steady-state uni-axial strain rate
$e_o(=\sigma_0/\mathrm{E})$ Normalizing strain
$\lambda_{ij}(=\varepsilon_{ij}/e_o)$ Normalized strain tensor
$\dot{\varepsilon}_e(=2\dot{\varepsilon}_{ij}\dot{\varepsilon}_{ij}/3)^{1/2}$ Effective creep strain rate tensor

*Damage*

$\omega_1$ Dislocation strain softening damage parameter
$\omega_2$ Nucleation creep constrained cavity growth damage parameter
$\omega_3$ Continuum cavity growth damage parameter
$\omega_f$ Damage level at failure

*Material parameters*

$\varepsilon_f$ Creep failure strain
$E$ Young's modulus
$Q_s$ Activation energy for volume diffusion
$\rho_i$ Initial mobile dislocation density
$n$ Norton law creep index
$v$ Multi-axial stress rupture index
$d$ Grain size
$2\ell$ Cavity spacing
$f_h$ Grain boundary cavitated area fraction
$r_h$ Cavity radius
$A$, $B$, $C$, $D$, $M$, $P$, $Q$, $\beta$ Material constants

*Other parameters*

$\delta_{ij}$ Kronecker delta
$\Psi$ Energy dissipation rate potential
$H, \tilde{H}$ Unit step functions
$t$, $\tau$ Real time and normalized time
$\theta$ and $q$ Stress-state parameters for continuum cavity growth
$\tilde{\alpha}(=Q\sigma_0)$ Normalizing stress parameter
$\tilde{\sigma}(=\sigma/(1-\omega_2))$ Stress-damage term
$p(=(\omega_3)^{1/2}/(d/2\ell))$ Parameters for continuum cavity growth

## 1. Introduction

Modelling of high-temperature creep damage in metallic alloys has been done over a range of length scales, and a brief review is presented here for completeness. Onck and van der Giessen (1997a,b) proposed a 2-D micromechanics modelling method to study creep rupture mechanisms of polycrystalline materials using grain elements. The grain boundaries are described by interfacial elements that incorporate the dominant creep damage mechanisms, including cavity nucleation and growth at grain boundaries (Onck and van der Giessen, 1998; Nguyen et al., 2000a). Based on the physical mechanisms taking place at the microscopic length scale, the model addresses macroscopic intergranular creep crack growth. The physical length scales of grain size and grain boundary thickness are included in the computational model (Onck and van der Giessen, 1999; Nguyen et al., 2000b). The effectiveness of the approach can be confirmed by comparison of damage fields predicted from the micro-modelling techniques with experimentally determined distributions. Distributions of micro-cracks ahead of a macro-crack predicted using the micro-mechanics modelling technique of Nguyen et al. (2000b) compare well with those observed experimentally by Hayhurst et al. (1984a) in cracked copper plates loaded in plain strain tension. This research, when judged alongside the modelling performed at the grain scale by Dyson and McLean (1990) and by Cocks and Ashby (1982), shows the complementarity of multi-scale modelling approaches: work by Onck and van der Giessen (1999) at the micro scale; modelling by Dyson and McLean (1990) and by Cocks and Ashby (1982) at the micro- and meso-scale; and the Continuum Damage Mechanics (CDM) modelling reported here at the macro-scale. In the research presented here a macro-scale CDM approach is used which is informed by the results of grain or meso-scale models of Dyson and McLean (1990) and of Cocks and Ashby (1982).

Ashby and Dyson (1984) examined most of the physically-based creep deformation and damage rate equations that were developed prior to 1984 and reformulated them within the framework of CDM. They demonstrated that each damage micro-mechanism, when acting alone, results in a characteristic shape of creep curve. Although this put CDM on a physical basis and gave it a more extrapolative capability, Ashby and Dyson also recognized that this single state-variable approach is only an approximation, and that certain engineering alloys may require two (or more) damage variables to describe the creep damage behaviour adequately. For example, it has been proposed by Dyson and McLean (1990) that the long period of tertiary creep found in high ductility nickel-base superalloys is a consequence of the mobile dislocation density increasing with strain. However, the alloy fractures because of the gradual and parallel evolution of grain boundary cavitation which, in turn, will result in some additional coupling between this damage and creep strain rates.

A two-damage state-variable power law creep model, proposed by Dyson and Gibbons (1987) has been developed by Othman et al. (1993). The multi-axial creep constitutive equations make use of two features: firstly the sinh-function (Garafolo, 1965), to describe the stress sensitivity of damage and creep rates over a wide range of stress, for use in component analysis; and secondly, two-state variables to reflect the contributions to the softening process made by constrained cavity growth, and multiplication of mobile dislocations. These laws have been developed to describe the behaviour of nickel-base superalloys which are used in the fabrication of load-bearing and thermally-stressed gas turbine components. Computer modelling of the creep rupture behaviour, using these constitutive laws, has been carried out by Othman et al. (1994) for notched tension bars, and the results have been compared with experimental data reported by Dyson and Loveday (1981). It has been found from the experimental results that, at low stress levels ($\sigma_N \cong 0.2\sigma_y$ where $\sigma_N$ is the net section stress at the notch, and $\sigma_y$ is the material yield stress) damage evolution starts at the notch surface/root and progresses inwards towards the notch centre-line (outside-in failure), which is consistent with the computer modelling results using the physically-based two-damage variable sinh-constitutive equations. However, for the high stress levels ($\sigma_N \geqslant 0.5\sigma_y$), experimental results reveal that fracture initiates on the centre-line of the notch and progresses outwards to the notch surface (inside-out failure), and the conventional two damage variable constitutive models could not predict this creep rupture behaviour well (Othman et al., 1994).

The objectives of this paper are to: (i) predict the global failure response shown in the experiments on notched tension bars due to Dyson and Loveday (1981) i.e. for low stress, outside-in failure, and for high stress inside-out failure; (ii) identify the damage mechanisms occurring in nickel-base superalloys under high tri-axial

stressing; propose and calibrate the constitutive equations; (iii) make predictions of notch behaviour using the equations and the Finite Element Solver DAMAGE XX (Hayhurst et al., 1984b) and (Vakili-Tahami et al., 2005); and, (iv) compare predictions of failure strain and lifetimes made using finite element calculations and the two sets of constitutive equations with the experimental results of Dyson and Loveday (1981). The equations considered are based on softening due to multiplication of mobile dislocations, firstly combined with nucleation controlled creep constrained cavity growth; and, secondly combined with continuum void growth.

## 2. Damage mechanisms

Constitutive equations have been developed that reflect the physics of the softening processes taking place in tertiary creep. The equations incorporate two features: firstly, they make use of the sinh-function to describe the stress sensitivity of creep rates over a wide stress range; and, secondly, they make use of three-state variables to reflect the contributions to the softening process made by (i) multiplication of mobile dislocation; (ii) cavity nucleation and growth; and, (iii) continuum void growth.

All nickel-base superalloys undergoing creep – with the exception of those having very low strains to failure (less than 5%) – spend the majority of lifetime in the tertiary stage. This is also true when the stress is uni-axially compressive (Tilly and Harrison, 1973). That tertiary creep occurs equally in compression, as in tension, accords with the scalar nature of dislocation accumulation and is consistent with the operation of an intrinsic material mechanism rather than being a consequence of the type loading.

### 2.1. Softening due to multiplication of mobile dislocations

The micromechanism responsible for this generic behaviour is a progressive accumulation of mobile dislocations as creep proceeds (Dyson and McLean, 1983; Ashby and Dyson, 1984): it has been termed dislocation strain-softening and is shown schematically in Fig. 1a.

Creep in these materials is therefore not controlled by dislocation recovery but is best thought of in terms of the kinetics of dislocation multiplication and subsequent motion. By treating the velocity of dislocation around $\gamma'$ particles as one of diffusive drift, secondary and tertiary creep in these materials under variable uni-axial loading conditions can be shown (Dyson, 1988) to be represented by

$$\dot{\varepsilon}_1 = \dot{\varepsilon}_0(1-\omega_1)^{-1}\sinh(M\sigma_1), \quad \dot{\omega}_1 = C(1-\omega_1)^2\dot{\varepsilon}_1, \tag{1}$$

where $\sigma_1$ is the uni-axial applied stress giving the uni-axial strain rate $\dot{\varepsilon}$; $\dot{\varepsilon}_0 \propto \rho_i \exp(-(Q_s/RT))$; $Q_s$ is the activation energy for volume diffusion; $\rho_i$ is the initial mobile dislocation density; $M$ is a temperature and microstructurally sensitive parameter; and, $\omega_1$ is a damage parameter ranging between zero and unity that is defined by

$$\omega_1 = 1-(\rho_i/\rho). \tag{2}$$

The parameter $C$ reflects the propensity of the material for entering tertiary creep and its magnitude is inversely proportional to $\rho_i$. Since $\rho_i$ can be influenced by the material's processing route, the magnitude of $C$ is a sensitive indicator of the minor variations usually encountered in batch to batch dislocation substructure.

### 2.2. Softening due to void nucleation and growth

The second mechanism of grain boundary cavitation (Fig. 1b) is now discussed. Its presence or absence is strongly sensitive to alloy composition and processing route: for example, it is clearly absent in single crystals. Grain boundary cavitation is also a kinetic phenomenon and its influence on deformation resistance and on fracture mode under an arbitrary stress state depends critically on cavity nucleation rate and growth rate. When both parameters are large, relative to intrinsic deformation mechanisms, there is the potential for a strong coupling between the extent of cavitation and creep rate through the mechanism of creep-constrained cavity growth (Dyson and Loveday, 1981; Hutchinson, 1983; Anderson and Rice, 1984), leading to rapid tertiary creep and a low fracture ductility.

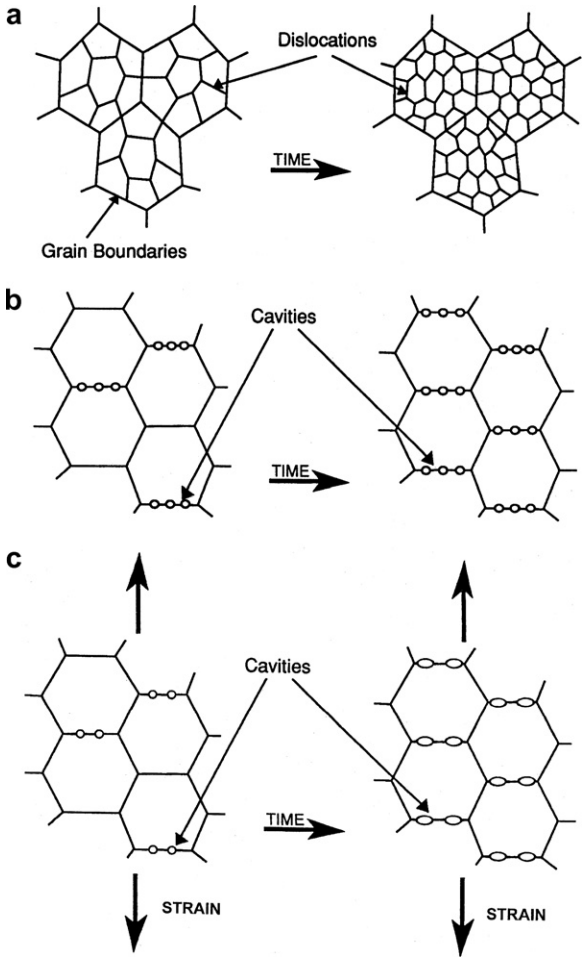


Fig. 1. Schematic representation of softening mechanisms of creep of superalloys: (a) multiplications of dislocation substructures; (b) grain boundary cavity nucleation and growth, (c) continuum cavity growth.

The damage parameter $\omega_2$ is defined as the area fraction of cavitation under creep constraint that is orthogonal to the maximum principal tension stress $\sigma_1$. The damage, $\omega_2$, represents grain boundary hole formation, or cavitation. Most commonly, the cavities appear on boundaries which lie roughly perpendicular to the maximum principal tensile stress direction (Ashby and Dyson, 1984). At low stresses, the damage, $\omega_2$, is in the form of spherical cavities and the material fails by the linkage of cavities which have grown by creep constrained cavity growth.

With dislocation strain-softening appropriate to superalloy behaviour the uni-axial strain rate response, as a function of $\omega_1$ and $\omega_2$, is given by:

$$\dot{\varepsilon}_1 = \dot{\varepsilon}_0 \sinh(\beta\sigma_1)/\{(1-\omega_1)(1-\omega_2)^n\}. \tag{3}$$

Creep constrained cavitation can either be nucleation or growth controlled; only nucleation control will be considered in this paper since this accords with the limited data in the literature. Using a nucleation rate model which is linear in strain rate, a failure criterion of $\omega_2 = \omega_f$ (all cavitated facets perpendicular to $\sigma_1$ are then essentially creep-constrained) gives:

$$\begin{aligned} &\dot{\omega}_2 = D\dot{\varepsilon}_1, \text{ or} \\ &\dot{\omega}_2 = \dot{\varepsilon}_1 \omega_f/\varepsilon_f, \end{aligned} \tag{4}$$

where $\varepsilon_f$ is the strain at fracture under uni-axial tension (Dyson, 1992), and $D = \omega_f/\varepsilon_f$.

Using Eqs. (3) and (4), the creep constitutive and damage evolution equations for axial strain rates in superalloys, derived from physical mechanisms by Othman et al. (1993), are given as

$$\begin{aligned}&\dot{\varepsilon}_1 = \dot{\varepsilon}_0 \sinh(\beta\sigma_1)/\{(1-\omega_1)(1-\omega_2)^n\},\\&\dot{\omega}_1 = C(1-\omega_1)^2\dot{\varepsilon}_1, \dot{\omega}_2 = \dot{\varepsilon}_1\omega_f/\varepsilon_f\end{aligned} \tag{5}$$

where $n$ is given by $n = \beta\tilde{\sigma}_1 \coth(\beta\tilde{\sigma}_1)$, where $\tilde{\sigma}_1 = \sigma_1/(1-\omega_2)$. The stress and damage level dependent value of $n$ reflects the change in slope of the log strain rate versus log stress curve for uni-axial creep data; and, the value of $n$ in Eq. (5) has been determined to describe this dependence.

### 2.3. Softening due to continuum cavity growth

The third mechanism of continuum void growth, shown schematically in Fig. 1c, is now considered. At elevated temperatures, the grain-boundary damage mechanism of nucleation controlled creep constrained cavity growth changes, at higher stresses, to the mechanism of continuum cavity growth. This damage mechanism dominates the fracture of the material (Dyson, 1992) at high stress under tri-axial stress conditions; and, the associated damage is quantified by the parameter $\omega_3$. A void can grow by power-law creep of the surrounding material which encompasses a grain boundary and the adjoining grain material (Hellan, 1975; Edwards and Ashby, 1979; Cocks and Ashby, 1982). The void growth-rate has been computed numerically (Needleman and Rice, 1980) or using bounding techniques (Cocks and Ashby, 1982). The latter approach yields analytical expression for strain rate and void growth rate. Application of the continuity equation to a grain boundary slab of material containing a void yields the following expressions, due to Cocks and Ashby (1982), for damage rate $\mathrm{d}f_h/\mathrm{d}t$ and strain rate $\dot{\varepsilon}_{ij}(=\mathrm{d}\varepsilon_{ij}/\mathrm{d}t)$

$$\begin{aligned}\frac{\mathrm{d}\varepsilon_{ij}}{\mathrm{d}t} &= \frac{3\dot{\varepsilon}_o}{2}\frac{S_{ij}}{\sigma_e}\sinh(Q\sigma_e)\left\{1+\frac{2r_h\theta}{\mathrm{d}}\left[\frac{1}{(1-f_h)^{\hat{n}}}-1\right]\right\}\\ \frac{\mathrm{d}f_h}{\mathrm{d}t} &= \dot{\varepsilon}_e\theta\left\{\frac{1}{(1-f_h)^{\hat{n}}}-(1-f_h)\right\}\end{aligned} \tag{6}$$

where

$$\hat{n} = Q\hat{\sigma}_e\coth(Q\hat{\sigma}_e), \quad \hat{\sigma}_e = \sigma_e/(1-f_h), \quad \sigma_e = (3\sigma_{ij}\sigma_{ij}/2)^{1/2}, \quad \dot{\varepsilon}_e = (2\dot{\varepsilon}_{ij}\dot{\varepsilon}_{ij}/3)^{1/2},$$

and where $r_h$ is the cavity radius, $d$ is the grain size; $Q$ is material constants for nickel-based superalloys; $f_h$ is the cavitated area fraction of a grain boundary; and the parameter $\theta$ has been determined by numerical techniques (Needleman and Rice, 1980) and by bounding methods (Cocks and Ashby, 1982) to be:

$$\theta = \tilde{H}\sinh\{q(J_1/\sigma_e)\} \tag{7}$$

where $q = \{2(\hat{n}-(1/2))/3(\hat{n}+(1/2))\}$; $J_1 = (\sigma_1+\sigma_2+\sigma_3)$ and $\sigma_1$, $\sigma_2$ and $\sigma_3$ are principal stresses; $\hat{n} = Q\sigma_e\coth(Q\sigma_e)$; and $\tilde{H}$ is a parameter to indicate the state of loading: for $J_1$ tensile, $\tilde{H}=1$; and for $J_1$ compressive, $\tilde{H}=0$. Whilst the original model of Cocks and Ashby (1982) includes dilatation, the present model assumes conservation of volume, this is an acceptable assumption up to the latter stages of tertiary creep.

At high stress levels, the timescales over which damage evolves by the nucleation controlled cavity growth mechanism are long compared to those for the multiplication of mobile dislocations and for continuum cavity growth. Hence, the mechanism of nucleation controlled cavity damage growth can be neglected at high stress levels. It is therefore necessary to combine the strain rate equation and the damage growth rate equation for softening due to continuum cavity growth, Eq. (6), with the damage rate equation for softening due to multiplication of mobile dislocations, Eq. (1), as follows:

$$\frac{d\varepsilon_{ij}}{dt} = \frac{3\dot{\varepsilon}_o}{2}\frac{S_{ij}}{\sigma_e}\frac{\sinh(Q\sigma_e)}{(1-\omega_1)}\left\{1+\frac{\theta p}{(1-\omega_3)^{\hat{n}}}-\theta p\right\}$$
$$\frac{d\omega_1}{dt} = C(1-\omega_1)^2\dot{\varepsilon}_e \tag{8}$$
$$\frac{d\omega_3}{dt} = \dot{\varepsilon}_e\theta\left\{\frac{1}{(1-\omega_3)^{\hat{n}}}-(1-\omega_3)\right\}$$

where $\omega_3 = f_h$; $p = (\omega_3)^{1/2}/(d/2\ell)$; $d$ is the grain size; and $2\ell$ is the cavity spacing.

In the next section, Eq. (5), for combined softening due to mobile dislocations and nucleation controlled cavity growth, which operates at low stress levels, and Eq. (8) for combined softening due to mobile dislocations and continuum cavity growth, which operates at high stress levels, are expressed in a normalized multi-axial form suitable for Continuum Damage Mechanics finite element studies of notched uni-axial tension bars.

## 3. Multi-axial forms and normalization of physics-based constitutive equations

In this section two sets of constitutive equations are developed for nickel-based superalloys for use at either low stress levels or high stress levels. They will then be used in CDM finite element studies of uni-axial constantly loaded Nimonic 80A notched tension bars at the temperatures of 750 °C (Dyson and Loveday, 1981).

### 3.1. Softening by multiplication of mobile dislocations and cavity nucleation and growth

#### 3.1.1. Uni-axial relations

The form of the constitutive equations proposed for uni-axial conditions are those given by Eq. (5) due to Othman et al. (1993), but modified using the unit function H to deal with a negative maximum principal stress. Thus

$$\dot{\varepsilon}_1 = A\sinh(B\sigma_1)/\{(1-\omega_1)(1-\omega_2)^n\},$$
$$\dot{\omega}_1 = CA(1-\omega_1)\sinh(B\sigma_1)/(1-\omega_2)^n, \tag{9}$$
$$\dot{\omega}_2 = DHA\sinh(B\sigma_1)/\{(1-\omega_1)(1-\omega_2)^n\}$$

where

$$A = \dot{\varepsilon}_0, \quad D = \omega_f/\varepsilon_f, \quad n = B\tilde{\sigma}_1\coth(B\tilde{\sigma}_1), \quad \text{and} \quad \tilde{\sigma}_1 = \sigma_1/(1-\omega_2).$$

#### 3.1.2. Multi-axial relations

The energy dissipation rate is described by the scalar function:

$$\psi = (A/B)\cosh(B\sigma_e)$$

where $\sigma_e^2 = \{3\tilde{S}_{ij}\tilde{S}_{ij}/2\}$, $\tilde{S}_{ij}$ is the deviator stress tensor given by

$$\tilde{S}_{ij} = \sigma_{ij} - \delta_{ij}\sigma_{kk}/3,$$

$\delta_{ij}$ is the Kronecker delta and $\sigma_{kk}$ obeys the summation convection. The strain rate Eq. (9) with zero damage then becomes

$$\frac{d\varepsilon_{ij}}{dt} = \dot{\varepsilon}_{ij} = \frac{d\psi}{d\tilde{S}_{ij}} = \frac{3A\tilde{S}_{ij}}{2\sigma_e}\sinh(B\sigma_e). \tag{10}$$

Introduction of the two state damage variables and in Eq. (10) leads to

$$\frac{d\varepsilon_{ij}}{dt} = \dot{\varepsilon}_{ij} = \frac{3A\tilde{S}_{ij}}{2\sigma_e}\frac{\sinh(B\sigma_e)}{(1-\omega_1)(1-\omega_2)^n}. \tag{11}$$

Implicit in this formulation is the assumption of conservation of volume. This is accurate until the latter stages of tertiary creep when the material density is known to change by a small amount. By introduction of the following normalized terms

$$\lambda_{ij} = \varepsilon_{ij}/e_0, \quad \Sigma_{ij} = \sigma_{ij}/\sigma_0, \quad S_{ij} = \tilde{S}_{ij}/\sigma_0. \tag{12}$$

where $\sigma_0 = e_0 E$ and $E$ is the elastic modulus, the normalized time $\tau$ may be defined as

$$\tau = \int_0^t (EA/\sigma_0)\mathrm{d}t = (EA/\sigma_0)t = (A/e_0)t. \tag{13}$$

Eq. (11) and the last two expressions of Eq. (9) may be rewritten using these terms as

$$\begin{aligned} \mathrm{d}\lambda_{ij}/\mathrm{d}\tau &= 3S_{ij}\sinh(\alpha\Sigma_e)/\{2\Sigma_e(1-\omega_1)(1-\omega_2)^n\}, \\ \mathrm{d}\omega_1/\mathrm{d}\tau &= Ce_0(1-\omega_1)\sinh(\alpha\Sigma_e)/(1-\omega_2)^n, \\ \mathrm{d}\omega_2/\mathrm{d}\tau &= DHe_0\sinh(\alpha\Sigma_e)\{\Sigma_1/\Sigma_e\}^v/\{(1-\omega_1)(1-\omega_2)^n\}. \end{aligned} \tag{14}$$

where

$$\alpha = B\sigma_0; \tilde{\Sigma}_e = \tilde{\sigma}_e/\sigma_0; \quad \tilde{\sigma}_e = \sigma_e/(1-\omega_2); \quad n = \alpha\tilde{\Sigma}_e\coth(\alpha\tilde{\Sigma}_e); \quad \text{and,}$$
$$H = \begin{cases} 1 & \text{for } \sigma_1/\sigma_e > 0 \\ 0 & \text{for } \sigma_1/\sigma_e < 0 \end{cases}.$$

The stress state term $(\Sigma_1/\Sigma_e)^v$ has been included in the third line of Eqs. (9) and (14). Guidance for this has been provided from the limited data in the literature which quantifies the effect of stress state on cavity nucleation; and, the choice of $(\Sigma_1/\Sigma_e)^v$ is based on the work of Hayhurst (1972) and of Dyson and McLean (1977). But similar ideas have been expressed by Lonsdale and Flewitt (1978) and by Cane (1979). The material parameters selected in Eqs. (13) and (14) are those used by Dyson and Loveday (1981) for Nimonic 80A tested at 750 °C. They have also been used by Othman et al. (1993) and by Dyson et al. (1996) in studies of notch tensions bars. The values of the material constants $A$, $B$, $D$, $v$ and $\omega_f$ are taken from the work of Dyson and Loveday (1981) for statically determinate plain bar testpieces:

$$A = 2\times10^{-6}\,h^{-1}, \quad B = 0.016\,\mathrm{MPa}^{-1}, \quad C = 300, \quad D = 2, \quad v = 2, \quad \omega_f = 0.3 \quad \text{and} \quad E = 2\times10^5\,\mathrm{MPa};$$

and, for the kinematically determinate notch bar structure $D$ is taken to vary linearly from $D = 1.00$, at $\sigma_e = 425$ MPa, to $D = 2.31$, at $\sigma_e = 154$ MPa. This is discussed in detail in a following section.

### 3.2. Softening by multiplication of mobile dislocations and continuum cavity growth

The uni-axial form of these constitutive relationships is not presented here, since continuum cavity growth is a mechanism which is usually inoperative under uni-axial stress, but predominates under multi-axial stresses.

#### 3.2.1. Multi-axial relations

By using the same procedure followed in Eqs. (10) and (11), a set of creep constitutive equations with two damage state variables, $\omega_1$ and $\omega_3$, for tri-axial stressing can be written in the form:

$$\begin{aligned} \frac{\mathrm{d}\varepsilon_{ij}}{\mathrm{d}t} &= \frac{3P}{2}\frac{S_{ij}}{\sigma_e}\frac{\sinh(Q\sigma_e)}{(1-\omega_1)}\left\{1+\frac{\theta p}{(1-\omega_3)^{\hat{n}}}-\theta p\right\} \\ \frac{\mathrm{d}\omega_1}{\mathrm{d}t} &= PC(1-\omega_1)\sinh(Q\sigma_e)\left\{1+\frac{\theta p}{(1-\omega_3)^{\hat{n}}}-\theta p\right\} \\ \frac{\mathrm{d}\omega_3}{\mathrm{d}t} &= P\theta\frac{\sinh(Q\sigma_e)}{(1-\omega_1)}\left\{1+\frac{\theta p}{(1-\omega_3)^{\hat{n}}}-\theta p\right\}\left\{\frac{1}{(1-\omega_3)^{\hat{n}}}-(1-\omega_3)\right\}, \end{aligned} \tag{15}$$

where $P = \dot{\varepsilon}_0$, is material constants for nickel-based superalloys.

*3.2.2. Normalization*

The normalized parameter defined by Eqs. (12) and (13) for strain, stress and time, carry over directly here; and, Eq. (15) can be written using these terms:

$$\begin{aligned}
\frac{d\lambda_{ij}}{d\tau} &= \frac{3}{2}\frac{\bar{S}_{ij}}{\Sigma_e}\frac{\sinh(\tilde{\alpha}\Sigma_e)}{(1-\omega_1)}\left\{1+\frac{\theta p}{(1-\omega_3)^{\hat{n}}}-\theta p\right\}\\
\frac{d\omega_1}{d\tau} &= Ce_0(1-\omega_1)\sinh(\tilde{\alpha}\Sigma_e)\left\{1+\frac{\theta p}{(1-\omega_3)^{\hat{n}}}-\theta p\right\}\\
\frac{d\omega_3}{d\tau} &= e_0\theta\frac{\sinh(\tilde{\alpha}\Sigma_e)}{(1-\omega_1)}\left\{1+\frac{\theta p}{(1-\omega_3)^{\hat{n}}}-\theta p\right\}\left\{\frac{1}{(1-\omega_3)^{\hat{n}}}-(1-\omega_3)\right\}\\
\theta &= \tilde{H}\sinh\{q(\tilde{J}_1/\Sigma_e)\},\tilde{J}=(\Sigma_1+\Sigma_2+\Sigma_3),\\
\tilde{\alpha} &= Q\sigma_0 \text{ and } \hat{n}=\tilde{\alpha}\hat{\Sigma}_e\coth(\tilde{\alpha}\hat{\Sigma}_e).
\end{aligned} \tag{16}$$

The normalized time variable may now be defined as in Eq. (13) as

$$\tau=\int_0^t (EP/\sigma_0)dt=(EP/\sigma_0)t=(P/e_o)t. \tag{17}$$

Calibration of the values of $P$ and $Q$ in Eq. (15) must be carried out to reflect behaviour at high stress under tri-axial stress states of the type found in notched tension bars. Calibration of $P$ and $Q$ is discussed in a subsequent section.

*3.3. Role of Tri-axiality in both Models*

In equation set (14), for softening by the combined mechanisms of multiplication of mobile dislocations and of nucleation controlled creep constrained cavity growth, the multi-axiality is given by the term $(\sum_1/\sum_e)^v$ in the third equation. Here it is the maximum principal tension stress which predominates. In contrast, for softening by the combined mechanisms of mobile dislocations and continuum cavity growth, given by Eq. (16), the multi-axiality is given by the term $\theta=\tilde{H}\sinh\{q(\tilde{J}_1/\sum_e)\}$ which appears in all three of the governing equations. Here it is the normalised first stress invariant $\tilde{J}_1$ which predominates. Hence it is expected that in the high tri-axial stress field of the axi-symmetric notched tension bar, when the levels of applied load are high, that softening due to continuum cavity growth will predominate over the $\sum_1$ controlled nucleation controlled creep constrained cavity growth mechanism.

## 4. Numerical procedures

A Continuum Damage Mechanics (CDM) finite element solver, DAMAGE XX (Hayhurst et al., 1984b) and (Hayhurst et al., 2005), was used for the numerical computations. The numerical procedure used to solve the boundary value problem for creep deformation and damage evolution was that used by Hayhurst et al. (1984b). It is based on the finite element method and employs constant strain triangular axi-symmetric finite elements. The procedure takes the elastic solution as its starting point and integrates with respect to the normalized time, the normalized creep strains, $\lambda_{ij}$, and creep damage variables $\omega_1$ and $\omega_2$ for combined softening due to dislocation multiplication and nucleation controlled cavity growth, and $\omega_1$ and $\omega_3$ for combined softening due to dislocation multiplication and continuum cavity growth. The integration is carried out over a series of discrete normalized time steps using a fourth order Runge–Kutta technique; this procedure involves the repeated solution of the boundary value problem to determine the field quantities required for the numerical solution. Creep damage, as represented by the two damage state variables, develops monotonically with time throughout the structure, and failure of an element is deemed to have occurred when the damage state variables, $\omega_2$ and $\omega_3$ attain the values of 0.5 and $\pi/4$, respectively. Material elements are then unable to transmit or sustain load and they are removed from the model. In the case of nucleation controlled creep constrained cavity growth the failure condition of $\omega_2=\omega_f=0.5$ has been selected for the notched bar, rather

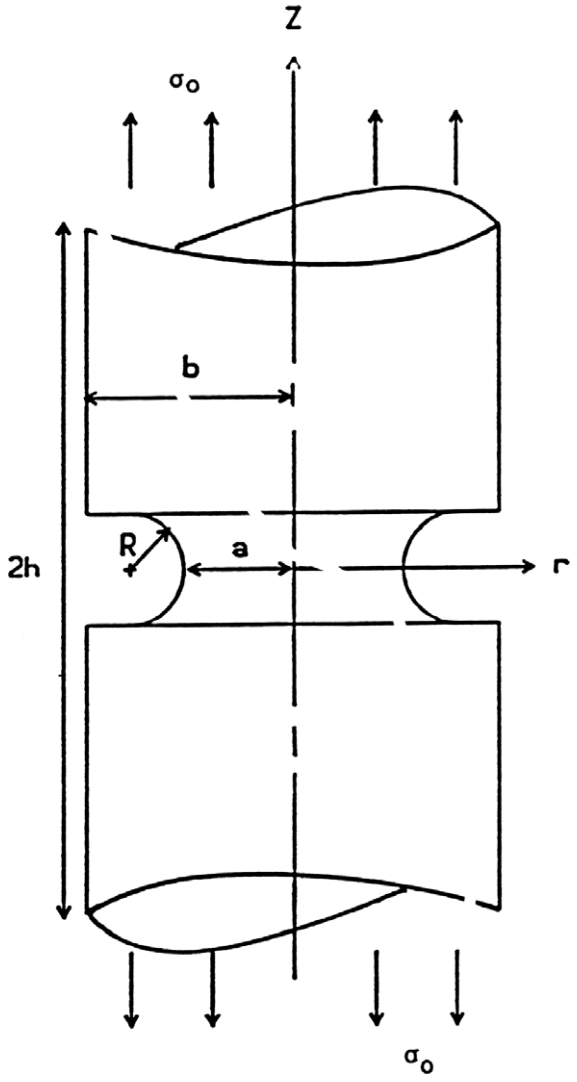


Fig. 2. Definition of loading conditions and geometry of the axi-symmetrically notched tension bar studied. $B/a = 1.9$, $R/a = 0.5$, $h/b = 3$, where $h$ is the length of the bar modelled and $\sigma_0$ is the uniform remote boundary stress.

than the value of $\omega_2 = \omega_f = 1/3$ taken for calibration with the uni-axial plain bar testpieces. This is because the plain bar behaves as a statically determinate structure, whereas the notched bar behaves as a kinematically determinate structure {i.e. a failing element has its displacement field determined by those of the surrounding unfailed elements}, and a higher value of $\omega_f$ is required to permit the stresses to redistribute to zero, prior to removal of an element, (Hayhurst et al., 2005) and (Mustata et al., 2006). In the case of ductile void growth, the failure condition $\omega_3 = \omega_f = \pi/4$ has been selected (Riedel, 1986) since the stress levels are high in the notched bar; and, once $\omega_3 = \pi/4$ has been achieved, then linkage of adjacent voids takes place catastrophically by time independent plastic collapse. The higher value of $\omega_f$ is required to permit complete stress redistribution in the constrained, tri-axial stress flow field. Following removal of an element, the boundary value problem is redefined to allow either a crack, or damage zone, to develop and spread. Once the boundary value problem has been redefined, the time integration is continued by taking the field variables just before the local failure occurred as the new starting point. The procedure is then repeated until complete failure of the cracked member occurs.

The geometry of the notched bar due to Dyson and Loveday (1981) is shown in Fig. 2. A single quadrant of the notched tension bar was selected for investigation. The quadrant was subdivided into triangular elements

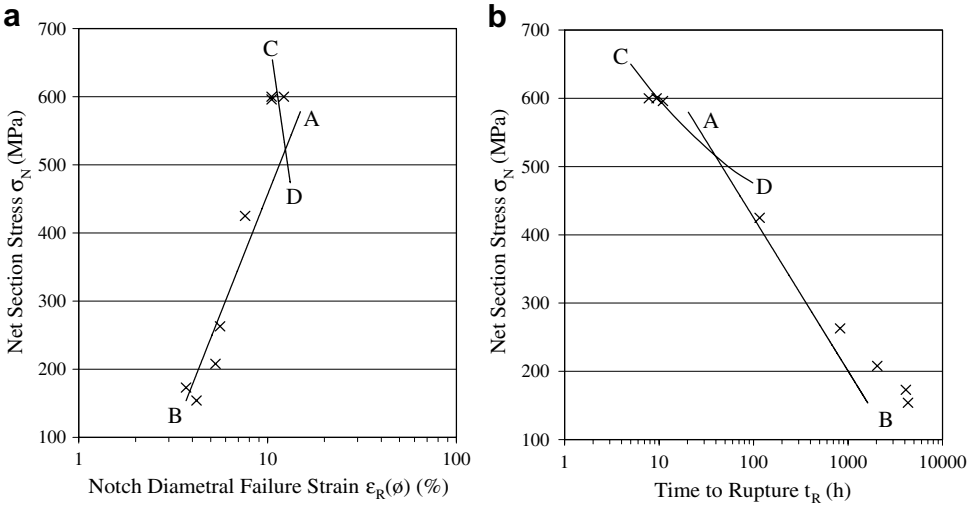


Fig. 3. Variation of notch diametral failure strain (a) and time to rupture of notched bar (b) with net section stress. The solid lines show predictions for nucleation controlled creep constrained cavitation (AB) and continuum cavity growth (CD); the symbols denote the experimental results of Dyson and Loveday (1981).

by the finite element mesh generation package, Femgen.[1] The size of these elements was redefined in the notched region of the bar, where a high level stress concentration occurs. A less well refined mesh was selected in the parallel portion of the testpiece where uniform stresses exist that change little over time. With regarding to the selection of the overall coarseness of the mesh it was acknowledged that damage finite element solutions can be critically mesh sensitive; and guidance was taken from previous investigations (Hayhurst et al., 1994; Dyson et al., 1996; and Vakili-Tahami and Hayhurst, 2007). Solutions were obtained with progressively refined meshes; and, whilst recognizing the need to have a minimum element size greater than approximately seven grain diameters to meet CDM requirements, the coarsest mesh was selected which gave lifetimes and temporal variations of damage fields that showed convergence and were acceptably repeatable. The mesh selected for the numerical investigation contains 642 constant strain triangular elements and 363 nodes for the notched bar. The half band width of the stiffness matrix was optimised to the minimum possible, using special purpose software to automatically re-number the element nodes. The procedure of optimising the band width of the stiffness matrix is important for the efficient usage of computer resources, and also to achieve accuracy of the numerical computations. The optimised mesh was then input into the Continuum Damage Mechanics Solver DAMAGE XX.

The loaded boundary of the mesh was subjected to a constant normalized stress $\Sigma_{zz} = 1$; and the boundaries of symmetry were subjected to the conditions $\Sigma_{rz} = 0$ and of zero normal displacement. The computations were carried out on a SUN workstation. The computed results of stresses, strains, displacements, damage state variables, were stored for subsequent examination by the postprocessor Femview.[1]

Finite element computations were carried out on the notched bar (Dyson and Loveday, 1981) with $\sigma_0$ as the stress at the outer boundary of the notched bar. For example, a value of $\sigma_0 = 166.2$ MPa is applied to produce an average axial stress at the notch throat of $\sigma_N = 600$ MPa. Presented in the next sections are the notched bar computer modelling results for: diametral notch strains at failure, $\varepsilon_R(\phi)$; lifetimes, $t_R$; and, creep damage fields. Introduced first are the low stress predictions made with the nucleation controlled creep constrained cavity growth damage mechanism, these are followed by the high stress predictions for the ductile void growth damage mechanism.

[1] Femgen and Femview are tradenames of FEMSYS Ltd. (TNO DIANA BV). Schoemakerstraat 97, 2628 VK DELFT, The Netherlands.

## 5. Behaviour at low stress: predictions made using the nucleation controlled creep constrained cavity growth model

The results are presented in three sections: 5.1, diametral notch strains at failure, $\varepsilon_R(\phi)$, 5.2, lifetimes, $t_R$; and, 5.3, the creep rupture damage fields.

### 5.1. Predictions of notch diametral failure strain

The experimental results of Dyson and Loveday (1981) are presented as the $x$-symbols in Fig. 3a, where they are compared with the predictions made using Eq. (14) and the CDM finite element technique, denoted by the line AB. To achieve these results two requirements have been identified:

(a) That $\omega_f = 0.5$ be used to allow stress redistribution prior to element removal. This is not unexpected since other estimates for $\omega_f$ can be as high as $\pi/4$ for the same mechanism (Riedel, 1986).
(b) That the value of $D$ in Eq. (14) be permitted to vary with stress. This variation was assumed to be linear between $D = 1.00$, at $\sigma_e = 425$ MPa, and $D = 2.31$, at $\sigma_e = 154$ MPa. Fig. 3a shows that the correct trend is predicted for diametral failure strains $\varepsilon_R(\phi)$ when stresses are below $\sigma_N = 425$ MPa. An error of the order of 15–19% may then be observed.

### 5.2. Predictions of notch bar lifetimes

Predictions of lifetimes made using the constitutive parameters given at the end of Section 3.1, with the exception of $\omega_f = 0.3$ being replaced by $\omega_f = 0.5$, are presented in Fig. 3b. It is apparent that the predictions consistently underestimate the experimental lifetimes for values of $\sigma_N$ below 425 MPa. The predictions are of the order of 2.4 times lower than the experimental results. The indication is that the values of the constitutive parameters $A$ and $B$ are not optimal; the high slope of the line AB suggests that the stress level sensitivity, given by $B = 0.016$ is too strong. It is worth recalling here that these values are those used in previous investigations, as outlined at the end of Section 3.1. For the work of Othman et al. (1993) the values of $A$, $B$, $C$ and $D$ were rounded to comply with values arrived at from physics-based evaluations. For this reason the parameters have not been recalibrated.

### 5.3. Comparison of predicted damage fields at failure with micro-structural evidence

At lower stresses, $\sigma_N \leqslant 500$ MPa, the behaviour is dominated by nucleation controlled cavity growth. Predicted damage fields on a diametral plane of the notch throat are shown in Fig. 4a for $\sigma_N = 154$ MPa close to failure of the testpiece. High damage levels $0.4 \geqslant \omega_2 \geqslant 0.5$, which represent failure, are shown in the vicinity of the notch surface. The rectangular box region with side AB shown in Fig. 4a may be compared with the same region of the micrograph due to Dyson and Loveday (1981) shown in Fig. 4b. Both figures show clearly that grain boundary cavitation has initiated on the notch surface and that damage growth takes place from the notch surface/root inwards towards the testpiece centre line i.e. outside-in failure.

## 6. Behaviour at high stress: predictions made by the continuum void growth model

Before predictions can be made using this model, physical parameters have to be assigned for the nickel-based alloy Nimonic 80A at the temperature 750 °C. These are the normalized inverse cavity spacing $d/2\ell$; the normalized initial cavity size $\omega_{3i} = (r_{hi}/l)^2$; and the values of $C$, $P$ and $Q$. It is evident from Fig. 3 that there are a set of three constraints which have to be satisfied, these are: the notch diametral failure strain $\varepsilon_R(\phi)$, and the notch bar lifetime $t_R$ at the stress $\sigma_N = 600$ MPa must match the experimental data. And, since the experimental data at $\sigma_N = 600$ MPa does not fall on the lines AB, the predicted lines $\varepsilon_R(\phi)$ v $\sigma_N$, and $t_R$ v $\sigma_N$ for the high stress behaviour must intersect the lines AB at the same stress level. The selection of the five parameters $d/2\ell$, $\omega_{3i}$, $C$, $P$ and $Q$ is now addressed.

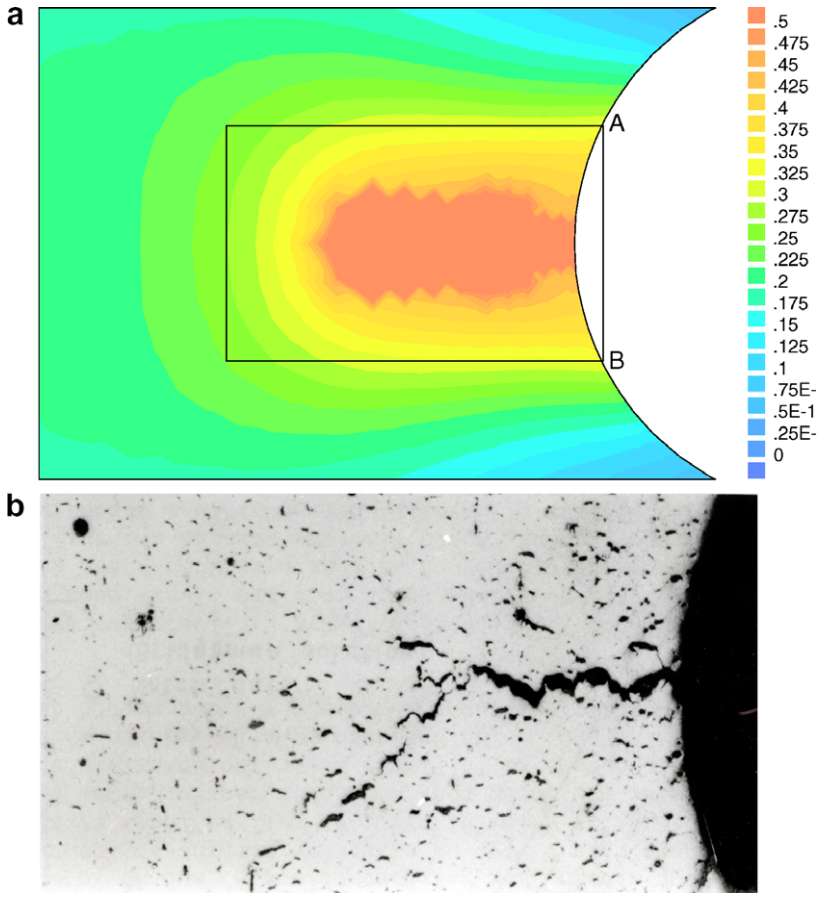


Fig. 4. Comparison of (a) predicted ($\omega_2$); and, (b) experimentally observed damage fields on a diametral plane at the notch throat, with $\sigma_N = 154$ MPa close to failure of the notch bar (Dyson and Loveday, 1981). The prediction is for damage due to: nucleation controlled, creep constrained cavitation, $\omega_2$; and, dislocation sub-structure softening, $\omega_1$. The figures are of different magnification, and the left-hand edge of (a) coincides with the notch bar centre-line; the micrograph, (b) has been taken of the region defined by the rectangle with vertical right-hand edge AB shown in (a).

### 6.1. Selection of constitutive parameter C

The parameter $C$ has been calibrated for Eq. (9), in particular: $\dot{\omega}_1 = C(1-\omega_1)^2\dot{\varepsilon}_e$, where $\varepsilon_e^2 = (2\varepsilon_{ij}\varepsilon_{ij}/3)$. Since the stress level sensitivity is embodied in the term $\dot{\varepsilon}_e$ it would be expected that the same value of $C = 300$ should hold at the higher stress levels. A value of $C = 300$ is therefore assumed.

### 6.2. Selection of the inverse cavity spacing d/2l

Rearrangement of the first and third equations of Eq. (16) yields an expression for $d\lambda_{ij}/d\omega_3$ which is weakly dependent on stress and independent of $\omega_1$. This reveals that the magnitudes of the failure strains $\varepsilon_R(\phi)$ are likely to be weakly dependent on $\sigma_N$; and, controlled by the initial damage or cavity size, $\omega_{3i}$, and the normalized inverse cavity spacing, $d/2\ell$. The grain size is given by Dyson et al. (1976) as $d = 20$ μm, and the inverse cavity spacing, as observed on typical failure surfaces (Pandey et al. (1985) and Zhang and Knowles (2002)) is of the order $d/2\ell = 6$. This value has been assumed here.

### 6.3. Strategy for the determination of P, Q and $\omega_{3i}$

Firstly the need to consider different values of $P$ and $Q$ for low and high stress levels is addressed i.e. $P \neq A$ and $Q \neq B$. It may be argued that $P$ an $Q$ should take identical values to $A$ and $B$ determined in Section 3.1 for

the combined mechanism of softening by multiplication of mobile dislocations and cavity nucleation and growth at stress levels below yield. However, preliminary investigations with $P = A$ and $Q = B$ reveal the inability of the model to predict the transition between low–high stress behaviour shown in the experimental data. In this way the acceptability of different values of $A$ and $B$ for low stresses, and of $P$ and $Q$ for high stresses may be justified because the applied stress levels are in excess of yield; and, the time-independent plastic strains for $\sigma_N = 600$ MPa are significant. The initial dislocation densities can therefore be expected to be different from those at lower stresses, and the stress level sensitivity to increase i.e. $Q > B$.

In this way it was recognized that there are three unknown parameters: $P$, $Q$ and $\omega_{3i}$; and, that three independent pieces of information are required to define them. The first is that the experimental lifetime $t_R = 8.5$ h, at $\sigma_N = 600$ MPa; the second is that the diametral strain at failure, $\varepsilon_R(\phi) = 11.3\%$ at $\sigma_N = 600$ MPa: and, the third is that the curves of $\varepsilon_R(\phi)$ v $\sigma_N$ and $t_R$ v $\sigma_N$ for both high and low stress behaviour (c.f. Fig. 3) intersect at the same stress level $\sigma_N \geqslant 500$ MPa. The procedure followed to satisfy these conditions is now described.

### 6.3.1. Selection of the initial values of P and Q

Sensitivity studies in which $P$, $Q$ and $\omega_{3i}$ were varied, revealed that the $t_R$ v $\sigma_N$ curve was weakly dependent on the value of $\omega_{3i}$, this observation was used in a two step procedure. The first step took as a starting point a value of $\omega_{3i} \approx 10^{-4}$; and following several iterations the values of $P$ and $Q$ were determined which gave the experimental lifetime of $t_R = 8.5$ h at $\sigma_N = 600$ MPa, and resulted in a line similar to CD (c.f. Fig. 3b) which intersected the line AB at a value of $\sigma_N \geqslant 500$ MPa.

### 6.3.2. Selection of the final values of P, Q and $\omega_{3i}$

The second step took these first estimates of $P$ and $Q$ and fixed them while $\omega_{3i}$ was varied to produce $\varepsilon_R(\phi)$ v $\sigma_N$ and $t_R$ v $\sigma_N$ curves of the type denoted by CD in Fig. 3a and b, respectively. Initial trials produced curves which either did not intersect with the lines AB, or intersected at different stress levels. Progressive iteration, and trial and error refinement, in which all three parameters, $P$, $Q$ and $\omega_{3i}$, were sequentially adjusted, yielded the following data set: $\omega_{3i} = 1 \times 10^{-5}$; $d/2\ell = 6$; $C = 300$; $P = 3.4 \times 10^{-8}\ \mathrm{h}^{-1}$; and $Q = 3 \times 10^{-2}\ \mathrm{MPa}^{-1}$.

This dataset was used to generate the lines in CD in Fig. 3a and b.

## 6.4. Comparison of predicted damage fields at failure with micro-structural evidence

Fig. 5a and b show predictions of the damage fields $\omega_1$ and $\omega_3$, respectively, on a diametral plane at the life fraction of $t/t_R = 0.83$ for $\sigma_N = 600$ MPa, i.e $t \approx 8.1$ h and $t_R \approx 9.7$ h. Fig. 5a shows the value of $\omega_1$ to have

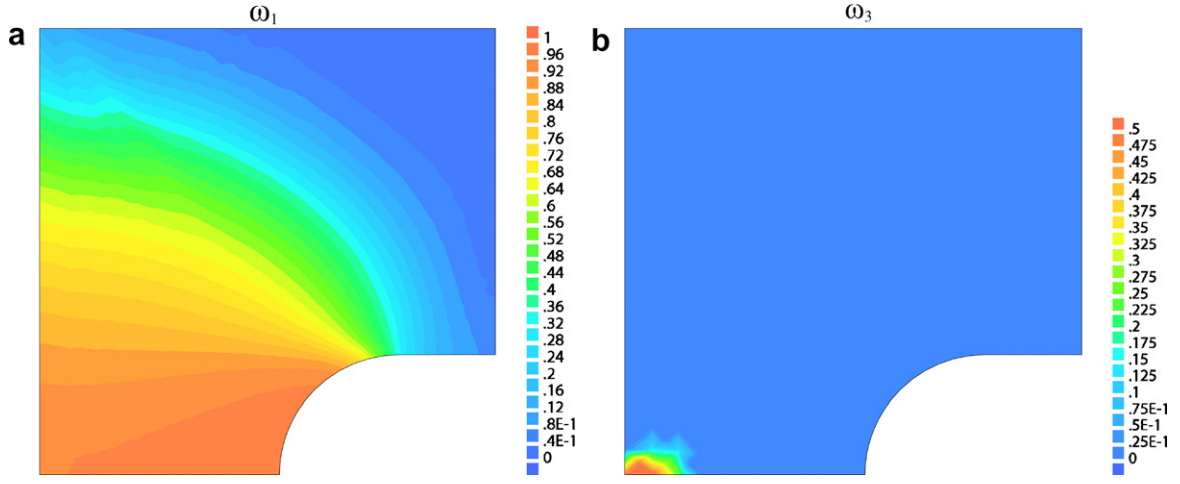


Fig. 5. Comparison of predicted damage fields on a diametral plane at notch throat with $\sigma_N = 600$ MPa, at the life fraction $t/t_R = 0.83$. The predictions are for (a) dislocation substructure, softening, $\omega_1$ and (b) damage due to creep continuum cavity growth damage, $\omega_3$. The $\omega_1$ damage field saturates across the notch throat at the life fraction $t/t_R = 0.83$.

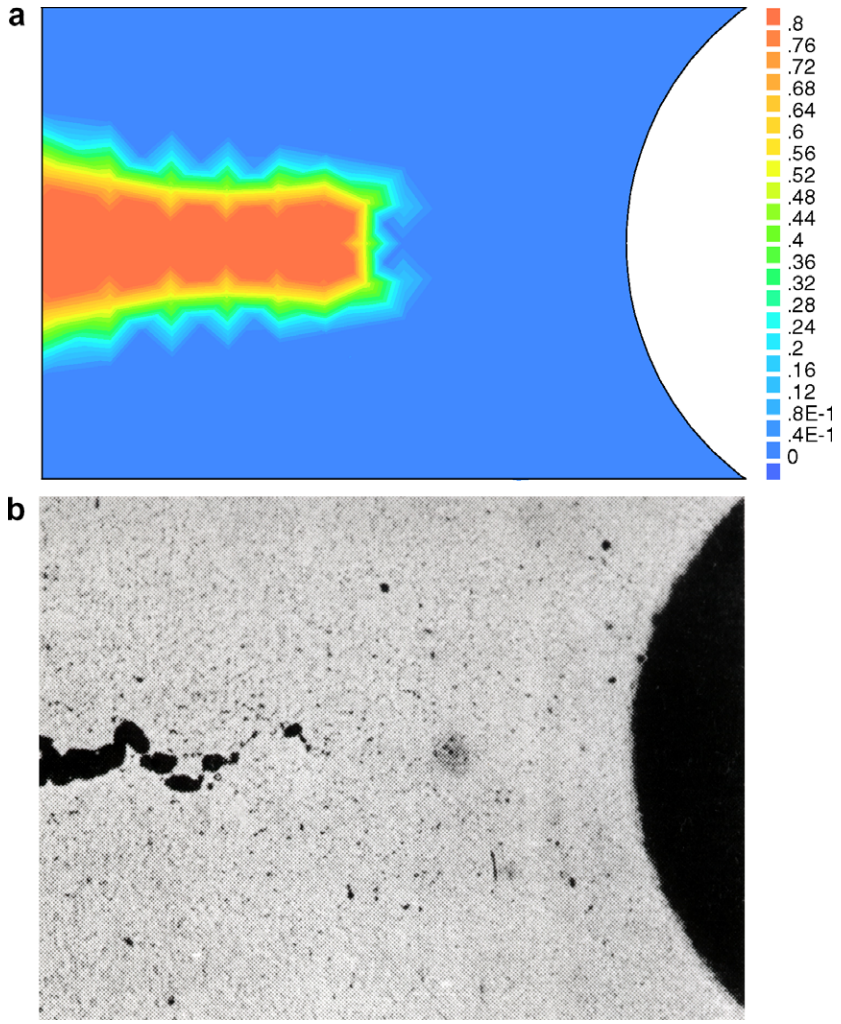


Fig. 6. Comparison of (a) continuum cavity growth damage ($\omega_3$) predicted using equation set (16); and, (b) experimentally observed damage fields on a diametral plane at the notch throat, with $\sigma_N = 600$ MPa, close to failure of the notch bar (Dyson and Loveday, 1981). Both figures are of the same magnification, and the left-hand edges coincide with the notch bar centre-line.

reached its saturation level across the notch throat. At this same time the field of $\omega_3$ is shown in Fig. 5b. Modest values of damage $\omega_3 \approx 0.5$ are concentrated on the centre-line of the bar at the notch throat. It is therefore evident that in the remaining 1.6 h, $\omega_3$ damage propagates across the notch section towards the notch root, to yield the pattern shown in Fig. 6a, close to failure of the testpiece. This reflects the very powerful stress-state influence on void growth and linkage. High levels of damage $\pi/4 > \omega_3 > 0.6$, which represent failure, are shown in Fig. 6 in the vicinity of the notch throat close to the testpiece centre-line. Fig. 6a may be compared with the same region in the micrograph due to Dyson and Loveday (1981) shown in Fig. 6b. Both figures show clearly that continuum cavity growth has caused damage evolution from the testpiece centre-line to the notch surface. Fracture is therefore caused by cavity nucleation and ductile void continuum growth (Dyson and Loveday, 1981) for $\sigma_N > 500$ MPa; and, the direction of damage growth shows inside-out failure.

### 6.5. Significance of initial cavity size or $\omega_{3i}$

A value of the initial damage level $\omega_3 = \omega_{3i} = 1 \times 10^{-5} = (r_{hi}/\ell)^2$, where $r_{hi}$ is the initial cavity radius following nucleation, was required to yield the results summarized in Fig. 3. Given that the ratio of the grain size to the cavity spacing $2\ell$ has been assumed to be $d/2\ell = 6$, and that $d$=20 μm, then the radius of the nucleated

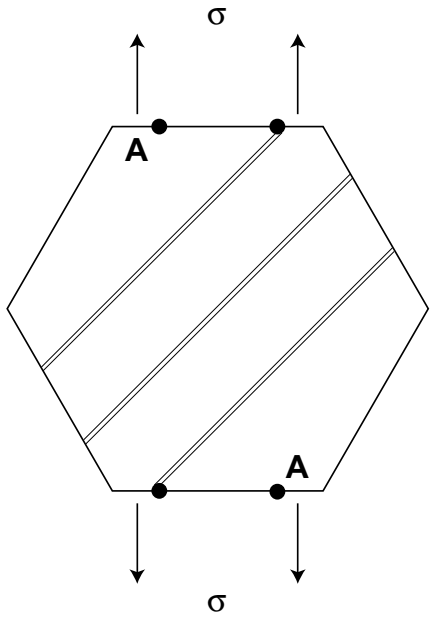


Fig. 7. Schematic of an isolated grain undergoing void initiation. Second phase particles/precipitates are intersected by slip bands of approximate width $10 \times 10^{-9}$ m. Voids are nucleated on particles/precipitates by de-cohesion, and subsequently grow by ductile void growth mechanisms.

void is $r_{hi} = 5.27 \times 10^{-9}$ m. This is of the order of one half of the thickness of a narrow slip band; and, a postulated mechanism for cavity initiation is shown schematically in Fig. 7. Here the slip bands intersect with second phase grain boundary particles/precipitates $A$; the stress levels, at 750 °C are not high enough to cause incoherency of $A$ with the matrix, as would be the case in fracture under monotonic loading; and, instead decohesion is postulated where the slip bands intersect with $A$. The radius of the nucleated void is of the order of half the slip band width. The voids then grow, in a stress-state sensitive manner, according to Eq. (16). This postulated mechanism would explain why high stress creep fracture surfaces (c.f. Pandey et al., 1985) have a similar appearance to those for high-temperature fast fracture under monotonic loading.

## 7. Discussion

The investigation has been motivated by experimental creep rupture data on uni-axially loaded notched bars carried out by Dyson and Loveday (1981). Two extreme failure modes were observed: one for low stress, showing failure propagation from the outside notch surface to the inside or centre-line of the testpiece; and, the second for high stress, showing failure propagation from the inside of the specimen to the outside of the notch surface. The objectives were to identify the physics of the processes responsible for this global response, rather than to focus on localized characteristics within the notch; and, to describe the global behaviour using physics-based constitutive equations, accepting the necessity to compromise some numerical accuracy.

Whilst the above objectives have been successfully achieved, it is evident that more test data is required at very high net section stresses $\sigma_N > 600$ if the high stress constitutive equations are to be calibrated directly with greater accuracy. Also in practical situations when engineering components are subjected to combined low–high load cycling, the highest stresses will most likely fall within the mid-range, where the two sets of constitutive equation will interact. However, test data for mid-range net section stresses $450 < \sigma_N < 550$ MPa was not available, and hence development of constitutive equations for these conditions would, at best, have been tenuous. Had such data been available, and a synthetic model developed for the entire stress range, it would have been desirable to check predictions against test results for an independent test geometry where stresses

operate at high levels, even for short times; e.g. a deeper notch with a sharper notch radius. However, due to the absence of such test data the development of a synthetic formulation has not been attempted.

## 8. Conclusions

1. The two constitutive equation sets have been shown to be capable of predicting the two different damage evolution directions: at low stress, damage growth from notch root towards the notch centre-line (outside-in failure); and, at high stress damage growth from the notch centre-line to the notch root, (inside-out failure).
2. Two sets of constitutive equations have been proposed: firstly for low notch stress behaviour, the combined softening by multiplication of mobile dislocations and cavity nucleation and growth; and, secondly for high notch stress levels, combined softening by multiplication of mobile dislocations and continuum cavity growth. With appropriate selection of constitutive parameters the respective equation sets accurately predict all of the respective features for both low and high stress behaviour. This includes lifetime, diametral failure strain and modes of damage evolution.
3. For the low stress nucleation controlled creep constrained cavity growth mechanism, it was necessary to allow the value of $D$ in Eq. (14) to vary with stress, in order to model the experimentally observed variation of uni-axial failure strain with stress level (Dyson and Loveday, 1981).
4. For the continuum ductile void growth model, it was found necessary to recalibrate Eq. (15) against the high stress notch bar experimental data, by adjusting the constitutive parameters $P$, $Q$ and $\omega_{3i}$, whilst maintaining $C$ at the value $C = 300$, for low stress behaviour. The value of the normalized inverse cavity spacing was assumed to be $d/2\ell = 6$. The value of $\omega_{3i} = 1 \times 10^{-5}$ was principally found to be necessary to predict diametral notch failure strains, and to a lesser extent notch bar lifetimes.
5. For the ductile void growth mechanism, the value of $\omega_{3i} = 1 \times 10^{-5}$ is equivalent to a void radius of $5.27 \times 10^{-9}$ m. A mechanism of void nucleation is postulated where a slip band of approximate width $10 \times 10^{-9}$ m intersects with second phase grain boundary particles/precipitates to cause decohesion and void nucleation.

## Acknowledgements

The authors gratefully acknowledge the continual interactions which have taken place during the course of this research with Prof. B.F. Dyson, Department of Materials, Imperial College, London. Also, the assistance of Dr. A.J. Pinkerton, School of MACE, The University of Manchester, with initial numerical studies using MATHEMATICA is gratefully acknowledged.

## References

Anderson, P.M., Rice, J.R., 1984. Constrained creep cavitation of grain facets. ACTA Metall. 33, 409.

Ashby, M.F., Dyson, B.F., 1984. In: Valluri, S.R. et al. (Eds.), . In: ICF Advances in Fracture Research, vol. 9. Pergamon Press, Oxford, pp. 3–30.

Cane, B.J., 1979. In: Miller, K.J., Smith, R.F. (Eds.), . In: Proc. Int. Conf. Mech. Behav. Mater., vol. 2. Pergamon Press, pp. 173–182.

Cocks, A.C.F., Ashby, M.F., 1982. On creep fracture by void growth. Prog. Mater. Sci. 27, 189–244.

Dyson, B.F., 1988. Creep and fracture of metals: mechanisms and mechanics. Rev. Phys. Appl. 23, 605–613.

Dyson, B.F., 1992. Material data requirements, creep damage mechanics and predictive models. In: Larsson, L.H. (Ed.), Proc. Int. Conf. High-Temp. Structural Des.. M.E.P. Publications, London.

Dyson, B.F., Gibbons, T.B., 1987. Tertiary creep in nickel-base superalloys: analysis of experimental data and theoretical synthesis. ACTA Metall. 35.9, 2355–2369.

Dyson, B.F., Hayhurst, D.R., Lin, J., 1996. The ridged uni-axial testpiece: creep and fracture predictions using large-displacement finite-element analyses. Proc. R. Soc. Lond. A 452, 655–676.

Dyson, B.F., Loveday, M.S., 1981. Creep Fracture in Nimonic 80A under Tri-axial Tensile Stressing. In: Ponter, A.R.S., Hayhurst, D.R. (Eds.), Creep in Structures. Springer-Verlag, Berlin, pp. 406–421.

Dyson, B.F., Loveday, M.S., Rodgers, M.J., 1976. Grain boundary cavitation under various states of applied stress. Proc. R. Soc. Lond. A 349, 245–259.

Dyson, B.F., McLean, M., 1990. Creep deformation of engineering alloys: developments from physical modelling. ISIJ Int. 30.10, 802–811.
Dyson, B.F., McLean, D., 1977. Creep of Nimonic 80A in torsion and tension. Metal. Sci. J. 11, 37–45.
Dyson, B.F., McLean, M., 1983. Particle-coarsening, $\sigma_0$ and tertiary creep. ACTA Metall. 31, 17–27.
Edwards, G.H., Ashby, M.F., 1979. Intergranular fracture during power-law creep. ACTA Metall. 27, 1505.
Garafolo, F., 1965. Fundamentals of Creep and Creep-Rupture in Metals, Macmillan Series in Materials Science. Springer, Berlin.
Hayhurst, D.R., 1972. Creep rupture under multi-axial states of stress. J. Mech. Phys. Solids 20, 381–390.
Hayhurst, D.R., Brown, P.R., Morrison, C.J., 1984a. The role of continuum damage in creep crack growth. Phil. Trans. R. Soc. Lond. A311, 131–158.
Hayhurst, D.R., Dimmer, P.R., Morrison, C.J., 1984b. Development of continuum damage in the creep rupture of notched bars. Phil. Trans. R. Soc. Lond. A311, 103–129.
Hayhurst, D.R., Dyson, B.F., Lin, J., 1994. Breakdown of skeletal sress technique for lifetime prediction of notched tension bars due to creep crack growth. J. Eng. Fracture Mech. 49 (5), 711–726.
Hayhurst, D.R., Hayhurst, R.J., Vakili-Tahami, F., 2005. CMD predictions of creep damage initiation and growth in ferritic steel weldments in a medium bore branched pipe under constant pressure at 590 °C using a 5-material weld model. Proc. Roy. Soc. Lond. (A) 461, 2303–2326.
Hellan, K., 1975. An approximate study of void expansion by ductility or creep. Int. J. Mech. Sci. 17, 369.
Hutchinson, J.W., 1983. Constitutive behaviour and crack tip fields for materials undergoing creep-constrained grain boundary cavitation. ACTA Metall. 31, 1079.
Lonsdale, D., Flewitt, P.E.J., 1978. In: Haasen, P., Gerold, V., Kostroz, G. (Eds.), Strength of Metals and Alloys. Pergammon Press, Aachen, p. 245.
Mustata, R., Hayhurst, D.R., Vakili-Tahami, F., 2006. CDM predictions of creep damage initiation and growth in ferritic steel weldments in a medium bore branched pipe under constant pressure at 590 °C using a 4 material weld model. Arch. Appl. Mech. 75, 475–495.
Needleman, A., Rice, J.R., 1980. Plastic creep flow effects in the diffusive cavitation of grain boundaries. ACTA Metall. 28, 1315.
Nguyen, B.-N., Onck, P., van der Giessen, E., 2000a. A homogenised microstructural approach to creep fracture. C.R. Acad. Sci. Paris: Damage, Fatigue, Rupture 328 (Series II b), 733–739.
Nguyen, B.-N., Onck, P., van der Giessen, E., 2000b. Crack-tip constraint effects on creep fracture. Eng. Fracture Mech. 65, 467–490.
Onck, P., van der Giessen, E., 1997a. Influence of microstructural variations on steady state creep and facet stresses in 2-D freely sliding polycrystals. Int. J. Solids Struct. 34 (6), 703–726.
Onck, P., van der Giessen, E., 1997b. Microstructurally-based modelling of intergranular creep fracture using grain element. Mech. Mater. 26, 109–126.
Onck, P., van der Giessen, E., 1998. Micromechanics of creep fracture: simulation of intergranular crack growth. Comp. Mater. Sci. 13, 90–102.
Onck, P., van der Giessen, E., 1999. Growth of an initially sharp crack by grain boundary cavitation. Mech. Phys. Solids 47, 99–139.
Othman, A.M., Hayhurst, D.R., Dyson, B.F., 1993. Skeletal point stresses in circumferentially notched tension bars undergoing tertiary creep modelled with physically-based constitutive equations. Proc. R. Soc. Lond. A 441, 343–358.
Othman, A.M., Hayhurst, D.R., Dyson, B.F., Lin, J., 1994. Continuum damage mechanics modelling of circumferentially notched tension bars undergoing tertiary creep with physically-based constitutive equations. ACTA Metall. Mater. 42.3, 597–611.
Pandey, M.C., Mukherjee, A.K., Taplin, D.M.R., 1985. Effects of tri-axial stress state on creep fracture in Inconel alloy X-750. J. Mater. Sci. 20, 1201–1206.
Riedel, H., 1986. Fracture at High Temperature. Springer Verlag.
Tilly, G.P., Harrison, G.F., 1973. Interpretation of tensile and compressive creep behaviour of two nickel alloys. J. Strain Anal. 8, 124–131.
Vakili-Tahami, F., Hayhurst, D.R., 2007. Failure of a welded pressure vessel due to creep: damage initiation, evolution and reheat cracking. Phil. Mag. 87 (28), 4383–4419.
Vakili-Tahami, F., Hayhurst, D.R., Wong, M.T., 2005. High-temperature creep rupture of low alloy ferritic steel butt-welde pipes subjected to combined internal pressure and end loadings. Phil. Trans. Roy. Soc. Lond. (A) 363, 2629–2661.
Zhang, Y.H., Knowles, D.M., 2002. Prestraining effect on creep behaviour of nickel based superalloy. Mater. Sci. Technol. 18, 917–923.